Dynamic Regulation of Innate Lymphoid Cell Development During Ontogeny

Tao Wu[1,3,7], Sijie Chen[2,7], Jie Ma[4,7], Xinyi Zhu[1,3,7], Maocai Luo[1], Yuanhao Wang[1], Yujie Tian[1], Qingqing Sun[1], Jianhong Zhang[1], Xiaohuan Guo[1], Xuegong Zhang[2,5,*], Yunping Zhu[4,*], Li Wu[1,3,6,8*]

[1]School of Medicine, Institute for Immunology, Tsinghua University, Beijing, 100084, China.

[2]Key Lab of Bioinformatics/Bioinformatics Division, TNLIST and Department of Automation, Tsinghua University, Beijing, 100084, China.

[3]Tsinghua-Peking Center for Life Science, Beijing, China.

[4]State Key Laboratory of Proteomics, Beijing Proteome Research Center, National Center for Protein Sciences (Beijing), Beijing Institute of Life Omics, Beijing 102206, China.

[5]School of Life Sciences, Tsinghua University, Beijing, 100084, China.

[6]Beijing Key Laboratory for Immunological Research on Chronic Diseases, Beijing 100084, China.

[7]These authors contributed equally

[8]Lead Contact

*Correspondence: zhuyunping@gmail.com (Y.Z.), zhangxg@tsinghua.edu.cn (X.Z.), wuli@mail.tsinghua.edu.cn (L.W.)

Graphical abstract

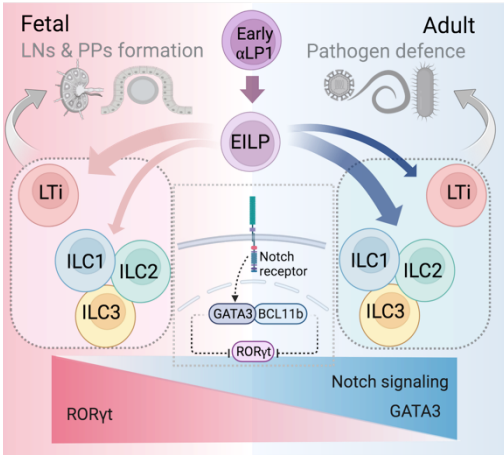

Highlight

- The ratio of LTi cells to non-LTi ILCs decreases from fetal to adult stage
- Different fate determination of ILC progenitors contributes to this decrease of LTi cell ratio during ontogeny
- Conserved trajectory from early αLPs to ILC precursors (ILCPs) during fetal

and adult ILC development

- Enhanced activity of Notch-GATA3 signaling in ILC precursors accounts for the transition of their differentiation from LTi cells in the fetal to non-LTi ILCs in adult.

SUMMARY

Dynamic composition of innate lymphoid cell (ILC) subsets in the small intestine during mouse ontogeny have been reported for more than ten years, but the underlying mechanisms remain incompletely understood. Here, we further confirmed a higher proportion of LTi cells in multiple tissues of fetal and new born mice, which decreased gradually with an increased proportion of non-LTi ILCs at the adult stage. Moreover, ILC progenitors showed a preferential differentiation towards LTi cells at the fetal stage, while at the adult stage, ILC progenitors differentiated mainly into non-LTi ILCs, consistent with the dynamic ILC subset composition from fetal to adult stages. However, through scRNA-seq analysis, we predicted a conserved trajectory of ILC development in the fetal liver and adult bone marrow, but the enhanced regulatory activity of Notch signaling and increased GATA3 expression in the adult-stage ILC progenitors, which suppressed RORγt expression, accounted for the transition from preferential LTi cell differentiation at the fetal stage to predominant non-LTi ILC differentiation at the adult stage. Accordingly, we propose a mechanism not described previously for the dynamic differentiation of ILC subsets, which may contribute to the dynamic change of ILC subset composition during ontogeny.

INTRODUCTION

Innate lymphoid cells (ILCs), representing the innate counterpart of T cells (Vivier et al., 2018; Walker et al., 2013), are widely distributed and contain mainly five subsets, NK cells, ILC1s, ILC2s, ILC3s and lymphoid tissue inducer (LTi) cells (Bal et al., 2020; Vivier et al., 2018). Upon activation, NK cells and ILC1s secret IFN-γ and mediate the defense to virus and intracellular bacterial infection. ILC2s secret IL-4/5/13 and mediate defense to parasite infection, and also promote allergy. ILC3s and LTi cells secret IL-17A/22, and mediate the defense to extracellular bacterial, thus keeping the local tissue homeostasis,

59 especially at the mucosal sites (Bal et al., 2020; Vivier et al., 2018). Meanwhile,
60 LTi cells are the major immune cells that induce the formation of secondary
61 lymphoid tissues, such as lymph nodes and Peyer's patches, mainly at the
62 embryonic stage (Eberl et al., 2004; Onder and Ludewig, 2018).
63 ILCs are majorly derived from common lymphoid progenitors (CLPs), and
64 extand through ILC-restricted $\alpha_4\beta_7^+$ lymphoid progenitors (αLPs) that can be
65 further defined as the early innate lymphoid progenitors (EILPs) (Yang et al.,
66 2015), common helper innate lymphoid progenitors (CHILPs) (Klose et al.,
67 2014) and innate lymphoid precursors (ILCPs) (Constantinides et al., 2014).
68 This series of progenitors is well defined in the adult bone marrow based on
69 their differentiation capacity (Lim and Di Santo, 2019; Vivier et al., 2018).
70 Interestingly, the composition of ILC subsets is dynamically changed
71 during mouse ontogeny. For instance, in the small intestine, $CD4^+$ LTi cells are
72 the dominant subset of RORγt$^+$ ILCs in the fetal stage, but gradually decreased
73 in composition after birth, which is accompanied with increased NCR^+ ILC3
74 (Sawa et al., 2010). Consistently, higher proportion of NCR^+ ILC3 is also found
75 in adult human tonsils than that in human fetal lymph nodes (Hoorweg et al.,
76 2012). In the thymus, LTi cells are also one of the dominant subsets at the
77 newborn stage but barely detectable in the adult thymus, meanwhile, ILC2s
78 become the dominant in the adult thymus (Jones et al., 2018). Although widely
79 concerned, the underlysing mechanisms of dynamic ILC subset composition
80 across tissues during ontogeny remain incompletely understood.
81 In this study, we found a higher propostion of LTi cells present in both
82 lymphoid (spleen) and non-lymphoid tissues (small intestine, colon, lung and
83 liver) at fetal and new born stage, and the LTi cell ratio decreased gradually
84 accompanied with an increased proportion of non-LTi ILCs at adult stage.
85 Consistent with this finding, ILC progenitor cells from fetal liver preferentially
86 differentiate into LTi cells, while those from adult bone marrow preferred to
87 differentiate into non-LTi ILCs. Interestingly, this alteration occurred within one
88 week after birth. We further identified a conserved ILC developmental pathway
89 from early αLPs to ILC precursors (ILCPs) in fetal liver and adult bone marrow
90 by scRNA-seq analysis, and confirmed that enhanced regulatory activity of
91 Notch signaling and increased GATA3 expression in the adult ILC progenitor
92 cells, which down-regulated RORγt expression, led to the shift in fate

determination of ILC subset from LTi cells in the embryonic stage to non-LTi ILCs in the adult. Taken together, our study proposesd the activity of Notch-GATA3 signalling as an regulator for the dynamic change of ILC development and ILC subset composition during mouse ontogeny.

RESULTS

Ratio of LTi cells to non-LTi ILCs decreases during ontogeny

To systemically investigate the ILC distribution during ontogeny, we examined the major ILC subsets in both lymphoid (spleen) and non-lymphoid tissues (small intestine, colon, lung, and liver), from mice at different ages. The dynamic composition of ILC subsets in all these tissues reached a stable state within two weeks after birth (Figure 1 and Figure S1). Based on the types of the dominant ILC subset in the adult stage, ILC distribution in these tisues can be classified into three distinct patterns: (1) ILC3s in the small intestine (Figure 1A and 1B); (2) ILC2s in the colon and lung (Figure 1D and 1E, Figure S1A and S1B); and (3) ILC1s in the spleen and liver (Figure 1G and 1H, and Figue S1D and S1E).

Despite the distinct tissue-specific distribution of the ILC subsets, a shared distribution feature was a higher percentage of LTi cells at the fetal and newborn stages, while a higher proportion of non-LTi ILCs, including ILC1s, ILC2s, and ILC3s, at the adult stage (Figure 1B, 1E and 1H, Figure S1B and S1E). Accordingly, the ratio of LTi cells to non-LTi ILCs was gradually decreased in all the tissues we examined and a stable state of this ratio was reached at around 2 weeks after birth (Figure 1C, 1F and 1I, Figure S1C and S1F), implicating some potential common regulatory mechanisms underlying the dynamic changes of ILC subsets during ontogeny.

Distinct progenitor differentiation capacity contributes to the composition shift of ILC subsets during ontogeny

In the analysis of ILC subset distribution across tissues, we also noticed a reduced percentage of γδ T cells and an increased proportion of αβ T cells during ontogeny (Figure S2). Considering the different ability of hematopoietic progenitors to generate γδ T cells and αβ T cells during embryonic and adult

124 stages (Yuan et al., 2012), and the close relationship between ILCs and T cells
125 (De Obaldia and Bhandoola, 2015), it is reasonable that fetal and adult
126 hematopoietic progenitors may also have different capacity of LTi cells and non-
127 LTi cells generation.

128 To address this question, we sorted the hematopoietic progenitor cells (LSK,
129 $CD45^{+}Lin^{-}c\text{-}Kit^{+}Sca\text{-}1^{+}$) from fetal liver and adult bone marrow respectively, for
130 the *in vivo* ILC differentiation assay. The progenies of LSKs in the small
131 intestines of the recipient mice were then analyzed 8 weeks later. Consistent
132 with previous studies (Yuan et al., 2012), we acquired a higher proportion of αβ
133 T cells among the progenies derived from adult LSKs (Figure S3A). In contrast,
134 higher proportions of ILCs and B cells, were noticed among the fetal LSK-
135 derived cells (Figure S3A). Although both embryonic and adult LSKs were able
136 to reconstitute all major ILC subsets (Figure S3B), lower proportion of LTi cells
137 while higher ILC1s and ILC2s were found among the ILCs derived from adult
138 LSKs (Figure S3B and S3C), thus, higher proportion of non-LTi ILCs (Figure
139 S3D). That was consistent with the gradually decreased ratio of LTi cells to non-
140 LTi ILCs during ontogeny.

141 To further compare the differentiation capacities of the fetal and adult ILC
142 progenitors, we isolated the LSKs, CLPs, and αLPs from fetal liver and adult
143 bone marrow respectively for *in vitro* differentiation assay. As expected, fetal
144 ILC progenitors preferentially generated LTi cells (Figure S4A and S4C), while
145 the adult counterparts produced more ILC1s and ILC2s, the non-LTi ILCs
146 (Figure S4B and S4D). We also observed that both fetal and adult αLPs were
147 more efficient in ILC differentiation, compared with LSKs and CLPs (Figure S4C
148 and S4D). The differentiation capacities of αLP1s and αLP2s were further
149 compared. Notably, an obvious population of NCR^{+} ILC3s was found among
150 the $ROR\gamma t^{+}$ ILCs derived from adult αLP2s, but few if any NCR^{+} ILC3s was
151 generated by fetal αLP2s, during both *in vitro* and *in vivo* differentiation assay
152 (Figure S5). Therefore, the composition of ILCs derived from fetal and adult
153 αLP2s could precisely reflected the distinct distributions of ILC subsets between
154 fetal and adult tissues.

155 We further confirmed that similar frequencies of CLPs, αLP1s and αLP2s
156 were maintained throughout the different stages during ontogeny (Figure 2A
157 and 2B). To identify when the differentiation capacity start to change, we sorted

158 αLP2 from fetal liver and bone marrow at different ages for *in vitro* differentiation
159 assay. Interestingly, bone marrow αLP2s from the mice within first week after
160 birth undergone significant changes in the differentiation ability, which gave
161 rising to a markedly decreased number of LTi cells and an increased number of
162 non-LTi ILCs, akin to the adult αLP2s (Figure 2C to 2F). This finding suggested
163 that changes in the differentiation capacity of ILC precursor cells occurred at
164 the neonatal stage, which was around one week earlier than the time when ILC
165 subsets composition reached a steady level in various tissues (at approximately
166 two weeks after birth) (Figure 1 and Figure S1). Therefore, the changed
167 differentiation ability of ILC precursors shortly after birth might account for the
168 dynamic changes of ILC subsets from the fetal to adulthood.

169 Single-cell transcriptomic landscape of fetal and adult ILC 170 progenitors

171 ILC progenitors are rare populations in both fetal liver and adult bone marrow,
172 particularly, fetal ILC progenitors have not yet been well illustrated, so we
173 isolated αLPs, containing both αLP1s and αLP2s, from fetal liver and adult bone
174 marrow for single-cell RNA sequencing (scRNA-seq) analysis, to further
175 compare the ILC development between these two stages. After strict quality
176 control (see quality control methods in the appendix), we selected 4284 fetal
177 and 3442 adult αLPs for further UMAP analysis. Ten distinct clusters were
178 revealed (Figure S6A) and all these cells expressed *Ptprc*, *Il7r*, *Itga4*, and *Itgb7*
179 (Figure S6B). Cluster 0, 1, 2, and more than half of cluster 6 showed high
180 expression of *Flt3*, represented αLP1s. The other clusters that did not express
181 *Flt3* represented αLP2s (Figure S6B).
182 Based on the expression characteristics of known transcription factors such
183 as *Id2*, *Tcf7*, and *Zbtb16*, we could define the clusters involved in ILC lineage,
184 i.e., Cluster 6, 3, 7, 8, 9, and 4, which were mainly distributed within αLP2s
185 (Figure S6B). Among them, Cluster 6, 3, and 9 were the progenitors at the early
186 stages during ILC development, as they expressed high level of *Tcf7*. Through
187 comparative mapping analysis of cell transcriptome, we also found that the
188 transcriptome of these early precursor cells shared some characteristics of T
189 cell precursors, such as ETP and DN T (Figure S6C). Among those, C6
190 expressed high *Nfil3* and low *Id2*, representing the early ILC progenitors (EILPs)
191 (Harly et al., 2019); the cells in C3 highly expressed *Zbtb16* and *Pdcd1*, the

specific markers for ILC progenitors (ILCPs) (Constantinides et al., 2014; Yu et al., 2016), they also expressed some signature genes of multiple ILC subsets, including *Gata3*, *Rora*, *Ccl5*, *Ltb, etc.*, we therefore defined C3 as ILCPs (Figure 3B). C7 also showed strong features of multiple ILC subsets, as well *Il18r1* (Figure 3B), the characteristic maker of ILCPs seeded in the peripheral tissues via circulation system (Zeis et al., 2020), suggesting that C7 could represent the later stage ILCP. Accordingly, we defined C3 and C7 as ILCP.1 and ILCP.2, respectively. C9 was distinguished by high expression of *Rorc*, *Cxcr5*, *Ccr6*, and *Ltb*, the markers for LTi precursors. In addition, C9 also highly expressed *Cd74*, *H2-Aa*, and *H2-Ab1*, which may be associated with the newly annotated MHC-II^{+} LTi cells (Hepworth et al., 2013; Lyu et al., 2022) (Figure 3B). Meanwhile, C4 showed high features of both LTi cells (*Ltb*, *Rorc*, etc.) and ILC2s (*Gata3*, *Rora*, etc.) (Figure 3B), which was also presented by the cell referring analysis (Figure S6C). Since C4 also showed low expression of *Tcf7* and *Il18r1* (Figure 3B), C4 might be a mixed cluster containing LTiPs and ILC2Ps at more terminal stage. We therefore defined C9 as an early stage LTiP.1 and C4 as LTiP.2/ILC2P. Finally, C8 was defined as NKPs based on their higher expression of *Eomes*, *Tbx21*, *Il2rb*, etc. (Figure 3B and S6C).

In contrast, the residual cells within clusters 0, 1, 2, and 5 that containing mainly αLP1s, did not exhibit significant genetic features of ILC lineage. C0 showed high expression of *Pbk* (Figure 3B), and a comparable fraction of C0 were transcriptionally similar to pro-B cells (Figure S6C), so we defined C0 as pro-B-like αLPs. Using the same strategy, we defined C1 as CDP-like αLPs due to their high expression of *Irf8*, *Tcf4*, *Ctsh*, *Ctsb*, *Siglech*, etc., and C2 as ETP-like αLPs due to their high expression of *Cd34*, *Lmo2*, *Egfl7*, etc. (Figure 3B and S6C). C5 exhibited high expression of genes shared by C0, C1, C2, and C6, and contained multiple cell types, representing the highest heterogeneity among all these clusters according to cell referring analysis (Figure 3B and S6C). Therefore, we defined C5 as the early αLPs.

Among the ten clusters identified, we observed that cells from fetal liver and adult bone marrow were evenly distributed, except for C4 (LTiP.2/ILC2P) (Figure 3C). Notably, fetal C4 referred to LTi cells, while adult C4 referred to ILC2, based on the cell referring analysis (Figure S6D), and we also noticed that fetal C4 showed higher expression of *Rorc*, *Cxcr5*, *Ccr6*, etc., presenting

226 the LTiP moiety (Figure S6E), while adult C4 exhibited higher expression of
227 *Rora*, *Gata3*, *Bcl11b*, *Il17rb*, etc., consistent with ILC2P (Figure S6G).
228 Therefore, we fine-tuned the annotation and defined fetal C4 as LTiP.2 (Figure
229 S6F), and adult C4 as ILC2P (Figure S6H).

230 RNA velocity analysis predictes a conserved ILC differentiation 231 trajectory in fetal liver and adult bone marrow

232 Considering the dramatically different capacity of ILC subsets generation by
233 fetal and adult ILC progenitors, it is possible that distinct development pathways
234 may exist between these two stages. To further address this question, we
235 predicted the differentiation trajectories in both fetal and adult αLPs by using
236 RNA velocity analysis.

237 Four relatively conserved differentiation trajectories for both fetal and adult
238 αLPs were predicted, all of which began at early αLP (C5) and pointed towards
239 pro-B-like αLP (C0, Path 0), CDP-like αLP (C1, Path 1), ETP-like αLP (C2, Path
240 2), and ILC lineage (C3, Path 3), respectively (Figure 3D to 3F). Interestingly,
241 an conserved ILC lineage (Path 3), which originated from early αLP (C5) and
242 extended through EILP (C6) and ILCP (C3), was found in both fetal liver and
243 adult bone marrow, however, ILC lineage (Path 3) was terminated as LTiP in
244 fetal liver, while as ILC2P in adult bone marrow (Figure 3D to 3F). That
245 suggested some important regulatory factors may have already altered from
246 fetal to adult ILC development, leading to the distinct progenies of ILC
247 progenitors through the seemingly conserved development pathway.

248 RORγt- and GATA3-biased gene programs in fetal and adult ILC 249 subset fates

250 To further compare the potential gene regulatory network between fetal and
251 adult ILC development, we tried to using the TSC analysis. Firstly, we selected
252 the representative cells among the four trajectories (Path 0 to Path 3) (Figure
253 4A), and then analyzed the gene expression dynamics on the pseudotime along
254 Path 3 from C5 to C3, thus, the ILC commitment path (Figure 4B). Consistent
255 with the conserved trajectories between fetal and adult ILC development, some
256 common characters of gene expression dynamics were identified, e.g. *Flt3*,
257 *Spi1*, *Irf8*, *Lmo2*, etc. were enriched in early stage of the pseudotime, which
258 were significantly decreased with further differentiation (Figure 4B). Then, the

expression of *Lck*, *Sox4*, *Tcf7*, and *Gfi1b* were induced, representing the initiation of ILC commitment from early progenitor cells, followed by the expression of *Tox*, *Id2*, and *Zbtb16,* representing the committed ILC progenitors (Figure 4B).

Interestingly, some inconsistencies in gene expression patterns were also observed between embryonic and adult stages. Particularlly, in embryonic stage, expression of *Rorc* was almost synchronous with *Tox* and *Id2*, while *Gata3* was expressed relatively later (Figure 4B and S7A). However, in the adult stage, it is the expression of *Gata3* that was almost synchronous with *Tox*, *Id2*, and *Zbtb16*, while the peak expression of *Rorc* was appeared relatively later (Figure 4B and S7B). Moreover, analysis of differentially expressed genes revealed higher expression of *Gata3* and *Bcl11b* in the adult clusters, especially in C6 (EILP) and C3 (ILCP), but higher *Id2* and *Rorc* among fetal clusters (Figure S8A). In addition, higher GATA3 expression in the adult ILCPs (C3: GATA3^{hi}TCF-1^{+} αLP2), and lower RORγt in the adult clusters (C9: RORγt^{hi} TCF-1^{+} αLP2) were further confirmed by flow cytometry analysis (Figure S8D to S8F). In line with this, we also found a gradually decreased RORγt expression in intestinal RORγt^{+} ILCs during ontogeny, which was nearly reduced by half in the adult (Figure S8G and S8H).

Notably, *Notch2* began to be expressed early in the embryonic ILC lineage (Path 3), and its expression level significantly decreased thereafter. In contrary, the expression of *Notch2* in the adult stage was synchronous with *Zbtb16* and *Gata3* (Figure 4B). In addition, *Rbpj*, the most important member down-stream Notch receptor, was also synchronously expressed with *Tox* and *Id2* during adult ILC commitment (Figure S7B), but was restricted in a short period during fetal ILC commitment (Figure S7A). Moreover, higher expression of *Notch1* and *Rbpj* in adult clusters was revealed by analysis of differentially expressed genes (Figure S8A), and higher Notch2 expression in adult αLPs was confirmed by flow cytometry analysis (Figure S8B and S8C). Gene set variation analysis (GSVA) also suggested highely enriched Notch signaling pathway in adult αLPs (Figure S9). Therefore, higher activity of Notch signaling existed during ILC development in the adult stage than that in the fetal stage.

Furthermore, through the Ternary plots analysis showing the expression of the aforementioned transcription factors and their target genes, we could

293 clearly see that more genes were regulated by RORγt in the embryonic stage,
294 while in the adult stage, they were obviously biased to be regulated by the
295 Notch signaling and GATA3 (Figure 4C). These data suggested that RORγt
296 may play a pivotal role as a key transcription factor during fetal ILC
297 development, whereas Notch signaling and GATA3 appears to be more
298 influential in modulating adult ILC development.

299 GATA3 and Bcl11b have been shown to be induced by Notch signaling (Ho
300 et al., 2009; Hosokawa and Rothenberg, 2021; Rothenberg, 2019), and they
301 could repress *Rorc* expression (Califano et al., 2015; Zhong et al., 2015).
302 During adult ILC commitment, we noticed high expression of *Gata3* and *Bcl11b*
303 (C6 and C3), closely following the high expression of *Notch1*, *Notch2*, and *Rbpj*
304 (C5), genes involved in Notch signaling. This was not that obvious during fetal
305 ILC development (Figure 4D). Moreover, there appeared to be an opposing
306 expression trend between *Gata3*/*Bcl11b* and *Rorc*. Higher *Gata3* and *Bcl11b*
307 expression were observed along with lower *Rorc* expression during adult ILC
308 commitment. In contrast, higher *Rorc* expression was found with lower *Gata3*
309 and *Bcl11b* during fetal ILC commitment (Figure 4D). Accordingly, through
310 *dynamo* analysis (Qiu et al., 2022), we further predicted a suppressive effect of
311 GATA3 and Bcl11b on *Rorc* expression, particularly in the adult ILCP (C3)
312 (Figure 4E and 4F). Therefore, we speculated that the enhanced Notch
313 signaling in adulthood might upregulate transcription factors such as GATA3
314 and Bcl11b, which, in turn, down-regulated *Rorc* expression (Figure 4G).

315 Enhanced activity of Notch-GATA3-signaling in the adult 316 suppresses the generation of LTi cells but promotes non-LTi ILCs

317 Considering the important role of Notch signaling, GATA3, and RORγt in ILC
318 development (Chea et al., 2016; Cherrier et al., 2012; Eberl et al., 2004; Possot
319 et al., 2011; Sanos et al., 2009; Vonarbourg et al., 2010; Yagi et al., 2014; Zhong
320 et al., 2015; Zhong et al., 2020), it is reasonable that the enhanced activity of
321 Notch-GATA3 signaling may involved in the altered ILC subset fate
322 determination from fetal to adult.

323 To address this question, we used the OP9-DL1 cell line, which provided
324 continuous ligands for activation of Notch signaling, in the ILC *in vitro*
325 differentiation assay. Consistent with the previous studies (Possot et al., 2011;
326 Wong et al., 2012), continuous activation of Notch signaling led to dramatically

327 increased proportion of ILC2s (Figure 5A), acompanied with dramatically
328 decreased proportion of LTi cells among the progenies of fetal ILC progenitors
329 (Figure 5B), and dramatically decreased proportion of ILC1s among the
330 progenies of adult ILC progenitors (Figure 5C). The proportion of ILC3s showed
331 no significant change during this process (Figure 5D). Thus, enhanced Notch
332 signaling promoted the generation of ILC2 but suppressed LTi cell generation.
333 This could also be the reason why the ILC lineage in the fetal liver ended with
334 LTiPs and in adult bone marrow with ILC2Ps, respectively (Figure 3D to 3F).
335 Moreover, the intervention of Notch signaling at early stages, such as CLP and
336 αLP1, showed a greater extent of ILC subsets alteration (Figure 5A to 5D). On
337 the other hand, blocking Notch signaling in αLP2s by DAPT could significantly
338 reduced their ability to differentiate into ILC3s, leading to the decreased
339 proportion of ILC3s and increased proportion of LTi cells, but had limited effects
340 on the generation of ILC1s and ILC2s (Figure S10).

341 To further evaluate the effect of the increased GATA3 expression on ILC
342 differentiation from fetal to adult stage, *Gata3* was overexpressed in fetal
343 hematopoietic stem/progenitor cells (HSPCs), these HSPCs were then
344 transferred into recipient mice for *in vivo* ILC differentiation. Amongst the
345 progenies of GATA3 overexpressing HSPCs, the porpportion of ILC2s was
346 significantly increased while the proportion of total RORγt^{+} ILCs was
347 dramatically decreased. Moreover, among the RORγt^{+} ILCs, increased
348 proportion of NCR^{+} ILC3s but decreased LTi cells was found upon *Gata3*
349 overexpression (Figure 5E to 5G). Furthermore, *Gata3* overexpression reduced
350 the expression level of RORγt in RORγt^{+} ILCs from the recipient small intestine
351 (Figure 5H and 5I), consistent with the negative regulatory effect of GATA3 on
352 *Rorc* expression (Figure 4E to 4G).

353 Moveover, the reduced RORγt expression, as shown in adult *Rorc*
354 heterozygous mice of both *Rorc*$^{Gfp/+}$ and *Zbtb16*^{Cre}*Rorc*$^{f/+}$ genotypes (Figure 5K
355 and 5L), led to decreased proportion of LTi cells among RORγt^{+}ILCs, but
356 siginicant increased proportion of NCR^{+}ILC3s (Figure 5J and 5N). However,
357 proportions of ILC1s and ILC2s showed no significant change in *Rorc*
358 heterozygous mice (Figure 5J and 5M). Accordingly, when further transferred
359 the LSKs from the adult *Rorc* heterozygous mice for *in vivo* ILC differentiation
360 analysis, we found a dramatically decreased proportion of total RORγt^{+}ILCs,

among which, proportion of LTi cells was also significantly decreased, while proportion of NCR$^+$ILC3s dramatically increased (Figure S11A and S11B).

In addition, we observed that NCR$^+$ILC3s appeared three days after birth in the small intestine of *Rorc*$^{Gfp/+}$ mice, significantly earlier than in the wild type mice (Figure S11C). This finding indicated an accelerated induction of NCR$^+$ILC3s in mice when RORγt expression level was halved. Indeed, an increased proportion of NCR$^+$ILC3 population was also generated by fetal liver αLPs from *Rorc*$^{Gfp/+}$ mice, compared to that derived from wild type fetal αLPs (Figure S11D and S11E). In additionn, increased proportion of NCR$^+$ILC3s and reduced LTi cells were also detected among the progenies of adult *Rorc* heterozygous αLP2s (Figure S11F and S11G). In contrast, when further overexpressed RORγt in adult hematopoitic stem/progenitor cells (HSPCs), we found a decreased proportion of NCR$^+$ILC3s and increased LTi cells among the progenies in the recipient small intestine, while the development of ILC1s and ILC2s were almost unaffected (Figure S11H to S11L).

Taken together, these data demonstrated a layer of molecular regulation of ILC differentiation during mouse ontogeny, by which a higher level of RORγt expression by fetal ILC progenitors was associated with a higher potential to generate LTi cells preferentially at fetal and neonatal stage. The enhanced Notch-GATA3 signaling in the ILC precursors at later developmental stage was associated with the decreased RORγt expression, which promoted the generation of non-LTi ILCs and suppressed LTi cell generation. Therefore, the dynamic changes in ILC subset fate determination during ontogeny may result from the dynamic chages in Notch signaling activity, GATA3 and RORγt expression from the fetal to adult.

DISCUSSION

ILCs have been known as an important member in the immune system that maintaines the tissue homeostasis, with different subsets mediating distinct immune response (Bal et al., 2020; Vivier et al., 2018). The dynamic change of RORγt$^+$ ILC subset composition in the mouse small intestine during ontogeny has been reported more than ten years ago (Sawa et al., 2010), as well as the ILC subsets in the thymus (Jones et al., 2018). However, how the ILC subset composition is dynamically regulated across tissues during ontogeny is still

394 imcompletely understood. In this study, we thouroghly analyzed the ILC
395 composition in multiple tissues and compared the differentiation capacity of ILC
396 progenitors in conjuction with scRNA-seq analysis of ILC progenitors in fetal
397 and adult mice. Our results revealed a preferential LTi differentiation at the fetal
398 stage while predominant non-LTi ILC differentiation at the adult stage, that was
399 consistent with the decreased ratio of LTi cell to non-LTi ILCs across tissues
400 during ontogeny, and supported the notion that different differentiation capacity
401 of ILC progeitors contributes to the dynamic ILC subset compostion during
402 ontogeny. Moreover, our results also suggested that enhaced Notch-GATA3
403 signaling and reduced RORγt expression account for the change of
404 differentiation capacity of ILC progenitors from fetal to adult.

405 It is interesting and reasonable that different subsets of ILCs are required
406 during various developmental stages. Remarkably, we and others have further
407 confirmed that LTi cells are more prevalent throughout the fetal and newborn
408 tissues, while increased proportion of non-LTi ILCs immediately after birth,
409 including ILC1s, ILC2s, and ILC3s. Given the essential role of LTi cells in the
410 early development of secondary lymphoid organs (Eberl et al., 2004;
411 Krishnamurty and Turley, 2020), mainly during the embryonic and newborn
412 stages (Onder and Ludewig, 2018), the higher proportion of LTi cells indicates
413 the body's prioritization of forming key secondary lymphoid tissues in
414 preparation for the impending immune defense after birth. However, after birth,
415 the dody has to face viarous pathogens directly, It has been shown that ILC3s
416 are required for safeguarding the lungs against bacterial pneumonia during the
417 neonatal period (Oherle et al., 2020). Therefore, non-LTi ILCs become critical
418 to defense against various pathogens (Eberl et al., 2015; Lim and Di Santo,
419 2019; Vivier et al., 2018), particularly during the early stages after birth, when
420 the T cell-mediated adaptive immune response is incompletely formed (Mao et
421 al., 2018). A better understanding of how the ILC subset composition is
422 dynamically regulated is necessary and important. Recent studies highlighted
423 the influence of local niches on this process (Lim et al., 2017; Oherle et al.,
424 2020; Zeis et al., 2020). For instance, a high concentration of AhR ligands in
425 the small intestine promotes the differentiation and proliferation of ILC3s while
426 restricts ILC2s expansion (Kiss et al., 2011; Lee et al., 2012; Li et al., 2018). In
427 the lung environment, ILC precursor cells are driven to differentiate into ILC2s,

428 however, it is not clear whether these progenitor cells are from neonatal or adult
429 sources (Ghaedi et al., 2020; Oherle et al., 2020; Zeis et al., 2020), and they
430 could not fully explain the phenomenon found in this study, wherein the ratio of
431 LTi cells to non-LTi ILCs systematically decreased across tissues during
432 ontogeny. Therefore, additional mechanisms involved in regulating the dynamic
433 changes of ILC subset composition need to be clarified.

434 It is well known that the characteristics of hematopoietic stem/progenitor cells
435 (HSPCs) changes during ontogeny from fetal liver to adult bone marrow
436 (Jassinskaja et al., 2017; Kim et al., 2007; Medvinsky et al., 2011; Yuan et al.,
437 2012). Fetal HSPCs show a higher capacity of γδ T cells generation, while adult
438 HSPCs show a higher capacity of αβ T cells generation (Yuan et al., 2012). In
439 accordance, a higher composition of γδ T cells is observed across fetal tissues,
440 while a higher proportion of αβ T cells is seen throughout adult tissues (Dunon
441 et al., 1997). In line with the widely shared regulatory mechanisms governing T
442 cell and ILC development, our findings also unveil a distinct capacity for
443 generating ILC subsets from fetal and adult hematopoietic progenitors.
444 Particularly noteworthy is the higher capacity for LTi cell generation by fetal
445 progenitors, as opposed to the greater capacity for non-LTi ILC generation by
446 adult progenitors. This pattern aligns with the systematic reduction in the ratio
447 of LTi cell to non-LTi ILC from the fetal to adult development. Therefore, we
448 propose that hematopoietic progenitors, exhibiting distinct differentiation
449 capacities for ILC subsets at different developmental stages, play a significant
450 role in driving the dynamic changes in ILC subset composition during ontogeny.

451 The developmental pathway of ILC progenitors is well-delineated in adult
452 bone marrow (De Obaldia and Bhandoola, 2015; Harly et al., 2019; Ren et al.,
453 2022; Vivier et al., 2018), but not very clear in fetal liver (Ishizuka et al., 2016).
454 Notably, the development of fetal and adult ILCs exhibits distinct sensitivities to
455 the deficiency of Notch signaling (Chea et al., 2016; Possot et al., 2011) and
456 Ikaros (Li et al., 2016; Schjerven, 2013), implying potential divergence in the
457 developmental pathways of ILCs between these two stages. Surprisingly, our
458 scRNA-seq analyses revealed a conserved differentiation trajectory of ILC
459 development during these two stages. Nonetheless, the progenitors identified
460 in fetal liver exhibited differentially expressed genes and distinct gene
461 regulatory networks. Remarkably, Notch signaling was enriched during adult

ILC development, marked by higher expression of *Gata3*, *Tcf7*, and *Bcl11b*. These transcription factors are known to be promoted by Notch signaing and are involved in ILC subset fate determination (Cherrier et al., 2018; Fang and Zhu, 2017). In particular, our findings, as well as those of others (Chea et al., 2016; Zhong et al., 2020), have confirmed that heightened Notch signaling activation and increased *Gata3* expression promote the differentiation of non-LTi ILCs while inhibiting LTi cell differentiation. Additionally, we have demonstrated that the reduced expression of RORγt in the adult, which may beattributed to the increased expression of GATA3 and Bcl11b (Califano et al., 2015; Zhong et al., 2020), promoted NCR^+ ILC3 differentiation while suppressed LTi cell generation. Therefore, we propose that enhanced Notch-Gata3 sgianling and diminished RORγt expression contribute to the altered differentiation capacity of ILC progenitors in adults.

Furthermore, Notch signaling also plays a role in determining the fate of αβ T cells and γδ T cells in a dose-dependent manner. Increased Notch signaling activity is necessary for the generation of αβ T cells, while it is not essential for γδ T cells (Ciofani et al., 2006; Garbe et al., 2006; Tanigaki et al., 2004). Taking into account the enhanced Notch signaling observed in adult ILC progenitors, which still maintain T cell differentiation capacity, exemplified by the early αLP1 cluster (C5) we identified, it is plausible that enhanced Notch signaling could serve as a common trigger for shifting differentiation capacity from LTi cells to non-LTi ILCs, and probably from γδ T cells to αβ T cells as well, during the transition from fetal to adult stages. However, the mechanisms underlying the modulation of Notch signaling strength during ontogeny remain unclear and warrant further investigation.

Collectively, our findinngs highlight the dynamic regulation of ILC subset fate determination by adjusting the activity of Notch-GATA3 signaling and RORγt expression, leading to the gradually decreased ratio of LTi cells to non-LTi ILCs from fetal to adult. This study propose an additional mechanism that altered differentiation capacity of ILC progenitors may coordinate with the environment cues to meet the demands of distinct ILC subsets in the body during mouse ontogeny.

Limitations of Study

Our study revealed a correlation between changes in the differentiation ability

of ILC progenitor cells and the dynamic composition of ILC subsets in tissues during ontogeny. However, direct evidence for the extent to which changes in differentiation ability contribute to the distribution of ILC subsets in peripheral tissues is lacking. While we demonstrated that the differentiation capacity of ILC progenitors changed as early as one week after birth, we were unable to determine definitively whether ILC progenitors from the bone marrow are still required for generating ILC subsets in peripheral tissues after birth. This consideration is particularly pertinent given the tissue-residence feature of ILCs in adults.

AUTHOR CONTIBUTIONS

T.W., S.C., and L.W. designed the study. T.W. performed the experiments and acquired data with assistance of X.Zhu. S.C. analyzed the single-cell RNA-seq data. Y.Z., J.M., and J.Z. provide the single-cell RNA-seq data. M.L. and Y.W. provided technical assistance. T.W., S.C., L.W. analyzed and interpreted the data. Manuscript was written by T.W. and L.W., and this study was supervised by L.W., Y.Z. and X.Zhang.

ACKNOWLEDGEMENTS

We thank Xiaoguang Li, Wenlong Lai, Yujie Tian, Yijun Zhang, Jiaoyan Lv, Xin Liu, Chao Wang, Zen Shi, Site Feng, Ning Wu and Jingjiao Wu for for administrative/support. We thank Qinli Sun from Dr. Chen Dong lab in this institute for providing the *Rorc* over-expression plasmid. We thank Dr. Yan Shi, Dr. Xiaoyu Hu and Dr. Wenwen Zeng for providing advice. Flow cytometry and cell sorting were carried out on IITU platforms. We also thank the assistance of Laboratory Animal Research Center of Tsinghua University. This study was supported by grants from the Ministry of Science and Technology of China (National Key Research Project 2019YFA0508502 and 2022YFC2505001 to L.W.; National Key Research Project 2020YFE0202200 to Y.Z. and J.M), the National Natural Science Foundation of China (Grants 91642207 and 31991174 to L.W.), the National Basic Research Center of China (82388101 to L.W.), China Postdoctoral Science Foundation (to T.W.) and Tsinghua-Peking Center for Life Sciences (to L.W. and T.W.).

DECLARATION OF INTERESTS

METHODS

KEY RESOURCE TABLE

RREGENT or RESOURCE	SOURCE	IDENTIFIER
Antibodies		
Anti-mouse CD45 BV605 (30-F11)	BioLegend	Cat# 103112
Anti-mouse CD45.1 BV605 (A20)	BioLegend	Cat# 110738
Anti-mouse CD45.1 BV711 (A20)	BioLegend	Cat# 110739
Anti-mouse CD45.1 V450 (A20)	BD Biosciences	Cat# 580520
Anti-mouse CD45.2 PE-Cy7 (104)	BioLegend	Cat# 109830
Anti-mouse CD45.2 APC (104)	BioLegend	Cat# 109814
Anti-mouse CD45.2 APC-Cy7 (104)	BioLegend	Cat# 109824
Anti-mouse CD45.2 FITC (104)	Thermo Fisher Scientific	Cat# 11-0454-85
Anti-mouse CD3ε FITC (145-2C11)	BioLegend	Cat# 100306
Anti-mouse CD4 BV711 (RM4-5)	BioLegend	Cat# 100550
Anti-mouse CD8α APC-Cy7 (53-6.7)	BioLegend	Cat# 100714
Anti-mouse TCR-β FITC (H57-597)	Thermo Fisher Scientific	Cat# 11-5961-85
Anti-mouse CD11b FITC (M1/70)	Thermo Fisher Scientific	Cat# 11-0122-85
Anti-mouse CD11c FITC (N418)	Thermo Fisher Scientific	Cat# 11-0114-85
Anti-mouse CD11b PerCP/Cy5.5 (M1/70)	BD Biosciences	Cat# 550993
Anti-mouse CD19 FITC (6D5)	BioLegend	Cat# 115505
Anti-mouse NK1.1 APC (PK136)	Thermo Fisher Scientific	Cat# 17-5941-82
Anti-mouse NKp46 PerCP-eF710 (29A1.4)	Thermo Fisher Scientific	Cat# 46-3351-82
Anti-mouse NKp46 PE-Cy7 (29A1.4)	Thermo Fisher Scientific	Cat# 25-3351-82
Anti-mouse Thy1.2 APC-Cy7 (30-H12)	BioLegend	Cat# 105328
Anti-mouse Thy1.2 APC-eFluor780 (53-2.1)	Thermo Fisher Scientific	Cat# 47-0902-82
Anti-mouse GATA3 eFluor660 (TWAJ)	Thermo Fisher Scientific	Cat# 50-9966-41
Anti-mouse RORγt PE (AFKJS-9)	Thermo Fisher Scientific	Cat# 12-6988-82
Anti-mouse CCR6 BV421 (29-2L17)	BioLegend	Cat# 129818
Anti-mouse c-Kit APC-Cy7 (ACK2)	BioLegend	Cat# 135136
Anti-mouse c-Kit BV605 (ACK2)	BioLegend	Cat# 135121
Anti-mouse c-Kit APC (ACK2)	Thermo Fisher Scientific	Cat# 17-1172-83
Anti-mouse CD127-biotin (A7R34)	Thermo Fisher Scientific	Cat# 1312721-82
Anti-mouse CD127-BV421 (A7R34)	BioLegend	Cat# 135024
Anti-mouse $\alpha_4\beta_7$ APC (DATK-32)	Thermo Fisher Scientific	Cat# 17-5887-82
Anti-mouse $\alpha_4\beta_7$ PE (DATK-32)	Thermo Fisher Scientific	Cat# 12-5887-83
Anti-mouse Flt3 PE (A2F10)	Thermo Fisher Scientific	Cat# 12-1351-82
Anti-mouse Flt3 BV421 (A2F10)	BioLegend	Cat# 135314
Anti-mouse CD25 BV711 (PC61)	BioLegend	Cat# 102049
Anti-mouse Notch1 PE (HMN1-12)	BioLegend	Cat# 130607
Anti-mouse Notch2 PE (HMN2-35)	BioLegend	Cat# 130707
Anti-mouse KLRG-1 BV605 (2F1/KLRG1)	BioLegend	Cat# 138419
Anti-mouse KLRG-1 APC (2F1/KLRG1)	BioLegend	Cat# 138412
Ki-67-PE-Cy7 (SolA15)	Thermo Fisher Scientific	Cat# 25-5698-82

Chemicals, peptides, and recombinant proteins		
Recombinant Murine IL-7	PeproTech	Cat# 217-17
Recombinant Murine SCF	PeproTech	Cat# 250-03
Recombinant Murine Flt3L	PeproTech	Cat# 250-31L
DAPT	Selleck	Cat# S2215
Collagenase Type III	Worthington Chemicals	Cat# CLS-3
Penicillin- Streptomycin (10,000 U/mL)	GIBCO	Cat# 15140122
Percoll	GE Healthcare	Cat# 17-0891-01
RPMI 1640	GIBCO	Cat# C22400500BT
HBSS	GIBCO	Cat# C14175500CP
Critical commercial assays		
Foxp3 transcription factor staining buffer set	Thermo Fisher Scientific	Cat# 00-5523-00
BioMag anti-Rat IgG	Bangs Laboratories	Cat# BM560
7-AAD	Thermo Fisher Scientific	Cat# 00-6993-50
Flexible viability dye eFulor506	Thermo Fisher Scientific	Cat# 65-0866-18
Rat Gamma Globulin	Jacksonimmuno	Cat# 012-000-002
Experimental Models: Organisms/Strains		
C57BL/6J mice	Jackson lab	Jax000664 Jax002014
Rorc$^{GFP/+}$ mice	Dr. Xiaohuan Guo	N/A
Rorc$^{-/-}$*Il2rg*$^{-/-}$ mice	Dr. Xiaohuan Guo	N/A
Zbtb16^{Cre} mice	Dr. Xiaohuan Guo	N/A
Rorc$^{f/+}$*Zbtb16*^{Cre} mice	Dr. Xiaohuan Guo	N/A
OP9 cell line	Dr. Xiaohuan Guo	N/A
OP9-DL1 cell line	Dr. Xiaohuan Guo	N/A
pMSCV[Exp]-mGata3[NM_008091.3]:IRES:EGFP	VectorBuilder	
Software and algorithms		
FACS Diva software	BD Biosciences	
FlowJo V9.9.3 software	TreeStar	
GraphPad Prism 7.0 software	GraphPad	

528 ## RESOURCE AVAILABILITY

529 **Lead contact**

530 Further information and requests for resources and reagents should be directed to and will
531 be fulfilled by the lead contact, Li Wu (wuli@tsinghua.edu.cn).

532 **Materials availability**

533 This study did not generate any new unique reagents.

534 **Data and code availability**

535 Single-cell RNA-seq data have been deposited at GSA with the accession number
536 CRA011319.

537 ## EXPERIMENTAL MODEL AND SUBJECT DETAILS

538 **Animals and ethics statement**

539 CD45.2 mice (Jax000664) and CD45.1 mice (Jax002014) were obtained from Jackson
540 Laboratory. CD45.1.2 mice were generated by crossing CD45.2 mice (Jax000664) and CD45.1
541 mice (Jax002014). *Rag2*$^{-/-}$*Il2rg*$^{-/-}$ mice, *Rorc*$^{GFP/+}$ mice, *Zbtb16*^{Cre} mice, *Rorc*$^{f/+}$*Zbtb16*^{Cre} mice
542 were kindly provided by Dr. Xiaohuan Guo (Tsinghua University, Beijing, China). Mouse
543 embryos and pups were obtained by in-house breeding. Age of mice were illustrated in
544 indicated experiment. Fetal liver were collected at embryonic day 15.5 (E15.5) or E16.5.
545 For adult bone marrow analysis, 8- to 12-week-old mice were used. Mice after two weeks
546 old were sex-matched, while the male and female fetus or newborn mice were randomly used.
547 All mice used in this study were bred on a C57BL/6 background, and maintained in a specific
548 pathogen free (SPF) animal facility (12 h light and 12 h dark) at Tsinghua University. Animal
549 procedures were under the approval of the Institution Animal Care and Use Committee at
550 Tsinghua University.

551 ## METHOD DETAILS

552 **Cell preparation**

553 Single-cell suspensions of bone marrow, fetal liver, small intestine, colon, lung, spleen and
554 liver were prepared following the listed protocols for flow cytometry analysis and/or cell
555 sorting.

556 For progenitor enrichment from bone marrow, procedures were detailly described
557 elsewhere (Manz et al., 2001; Wu et al., 2001). Briefly, bone marrow cells were enriched
558 by red blood cell removing, density gradient centrifugation (1.086 g/ml Nycodenz), and
559 immunomagnetic depletion of the lineage positive cells labeled by markers of CD3, CD2,
560 CD8, CD19, B220, Mac-1, Ly6G and Ter119. For cell isolation from fetal liver, fetal liver
561 was collected from E15.5 or E16.5 fetus and repeatedly blew by 1 ml pipette tip, cell
562 suspensions were passed through a 70 μM strainer, further enriched by red cell removing
563 and density gradient centrifugation (1.086 g/ml Nycodenz), cells that lighter than 1.086
564 g/ml were collected and washed. These enriched cells were blocked by Rat IgG and further
565 stained with indicated antibody panel for CLPs (Lin^{-}CD127^{+}c-Kit$^{int/+}$Flt3^{+}$\alpha_4\beta_7^{-}$), αLP1s
566 (Lin^{-}CD127^{+}c-Kit$^{int/+}$Flt3^{+}$\alpha_4\beta_7^{+}$), αLP2s (Lin^{-}CD127^{+}c-Kit$^{int/+}$Flt3^{-}$\alpha_4\beta_7^{+}$).

567 For cell isolation from the small intestine and colon, the small intestine and colon were
568 flushed clean with cold mouse tissue PBS, opened along the longitudinal axis, and then
569 removed the Peyer's patches. The residual intestinal tissues were subjected to two
570 sequential 20-min incubated in 20 ml Buffer I (HBSS with 20mM EDTA, 10mM HEPES and
571 1M DTT), at 37°C with shaking (220 rpm), for the preliminary digestion. Peyer's patches
572 and mesenteric tissues were removed from the residual intestinal tissues that were further
573 incubated in 10 ml Buffer II (1640 RPMI + 10% FBS + 1mg/ml Collagenase III) for 60min

574 at 37°C with shaking (220 rpm), for final digestion. After which, samples were violently
575 vortexed, repeatedly blew by 1 ml pipette tips, and then passed through 70 μM strainer,
576 40% Percoll density gradient centrifugation was used for further immune cells enrichment.
577 The cells that heavier than 40% Percoll were washed and counted for further analysis.
578 For lung cell isolation, mouse lung tissues were minced and digested with collagenase
579 1A (0.5 mg/ml, Sigma) and Dnase I (0.05 mg/ml, Roche) in HBSS for 60 minutes at 37℃
580 in the thermostatic incubator, with several interval vortexes. Digested lung tissues were
581 further filtrated through a 70 μM strainer, the erythrocytes were removed by using red cell
582 removal buffer (0.168M NH_4CL), the residual cells were washed and collected for further
583 analysis.
584 For liver cell isolation from mice after birth, livers were collected and passed through a
585 100 μM strainer. The cells then enriched by density gradient centrifugation with 40%
586 Percoll, and red blood cells were removed. Splenocytes were isolated by forcing the
587 tissues through a 100 μM strainer, and red blood cells were further removed.

588 **Flow cytometry analysis and cell sorting**

589 Flow cytometry staining were performed in 96-well microtiter plates or 5 ml FACS tube.
590 Cells were blocked by Rat IgG and stained with fluorochrome-conjugated antibodies in
591 dark for 30-40 min on ice. Fixable Viability Dye eFluor506 or 7-AAD were used to exclude
592 the dead cells in all these samples. For intracellular transcription factor staining, cells were
593 fixed and permeabilized and stained with indicated antibodies using the
594 Foxp3/Transcription Factor Staining Buffer Set (Thermo Fisher Scientific). Data were
595 acquired on a BD LSRII or Fortessa cytometer, and cells were sorted by FACSAria III, in
596 the flow cytometry core at IITU.

597 ***In vitro* differentiation assay of ILC progenitors**

598 We cultured bone marrow progenitors (0.5-1×10^4/sample) from CD45.1 or CD45.2 wild
599 type mice, including CLP, αLP1, and αLP2, with total bone marrow cells (1×10^4/sample)
600 from CD45.1.2 wild type or CD45.2 *Rag2*$^{-/-}$*Il2rg*$^{-/-}$ mice as feeder cells in RPMI 1640
601 media supplemented with 10% fetal bovine serum, glutamine, β-mercaptoethanol,
602 penicillin, and streptomycin. For the OP9 and OP9-DL1 co-culture system, we sorted ILC
603 progenitors (500-1000 cells) and seeded them in wells with OP9 or OP9-DL1 cell lines
604 (500 cells for each well). All cultures were supplemented with stem cell factor (SCF, 100
605 ng/ml) and IL-7 (20 ng/ml), and ILC subsets among the daughter cells were analyzed 7-8
606 days later by flow cytometry.

607 **Adoptive transfer of ILC progenitors for in vivo differentiation assay**

608 We sorted equal number (0.5~1×10^4 for one recipient) of indicated progenitor from fetal liver
609 (CD45.2 wild type) and adult bone marrow (CD45.1,wild type mice), and mixed them with
610 competitor cells (5×10^5 for one recipient, total bone marrow from CD45.1.2 wild type or CD45.2
611 *Rag2*$^{-/-}$*Il2rg*$^{-/-}$ mice) befor transferring them to the lethally irradiated mice (CD45.1.2 wild type
612 or CD45.2 *Rag2*$^{-/-}$*Il2rg*$^{-/-}$ mice, 5.5 Gy twice with a 3-hour interval). Neomycin (1 mg/ml) and
613 Polymycin (0.1 mg/ml) were added to the drinking water for 1~2 weeks.
614 For the *Rorc* over-expression experiments, we isolated adult bone marrow progenitors (Lin$^-$c-
615 Kit$^{int/+}$Sca-1$^+$) from wild type (CD45.1) or *Rorc*$^{Gfp/+}$ (CD45.2) mice were transduced them with
616 Rorc-GFP plasmid (*Rorc*^{OE}) or empty plasmid (*Rorc*^{NC}). For *Gata3* over-expression experiment,

617 we transduced progenitors from the fetal liver (Lin^{-}c-Kit$^{int/+}$Sca-1^{+}) with either Gata3-GFP
618 plasmid (*Gata3*^{OE}) or empty plasmid (*Gata3*^{NC}). After Successfully transduction, we sorted and
619 mixed the progenitors with competitor cells (5×10^5 for each recipient mice, total bone marrow
620 from CD45.2 *Rag2*$^{-/-}$*Il2rg*$^{-/-}$ mice) before transferring to the lethally irradiated mice (CD45.1.2
621 wild type, 5.5 Gy twice with a 3-hour interval). Neomycin (1 mg/ml) and Polymycin (0.1 mg/ml)
622 were added to the drinking water for 1~2 weeks. We analyzed cells in the recipient mice 5~6
623 weeks after transfer.

624 **Single-cell RNA-seq library preparation**

625 Single αLP cells were sorted by FACS from embryonic liver (E15.5~16.5) and adult bone
626 marrow. After the confirming of cell purity (above 95%) and the cell viability (above 85%)
627 after sorting, cells were further sent to 10×Genomics sequencing platform for single-cell
628 transcriptome sequencing (Annaroad Gene Technology(Beijing)Co., Ltd).

629 **Single-cell RNA-seq data analysis**

630 The analysis details and code are placed in the online material
631 (https://github.com/chansigit/ilcdev).

632 QUANTIFICATION AND STATISTICAL ANALYSIS

633 **Statistical Analysis**

634 GraphPad Prism 7 was used for statistical analysis with the specific tests and the number
635 of samples used for each analysis (n) shown in the figure legends.

636 ADDITIONAL RESOURCES

637

638 REFERENCE

639 Bal, S.M., Golebski, K., and Spits, H. (2020). Plasticity of innate lymphoid cell subsets. Nature
640 reviews Immunology *20*, 552-565.

641 Califano, D., Cho, J.J., Uddin, M.N., Lorentsen, K.J., Yang, Q., Bhandoola, A., Li, H., and Avram,
642 D. (2015). Transcription Factor Bcl11b Controls Identity and Function of Mature Type 2 Innate
643 Lymphoid Cells. Immunity *43*, 354-368.

644 Chea, S., Schmutz, S., Berthault, C., Perchet, T., Petit, M., Burlen-Defranoux, O., Goldrath,
645 A.W., Rodewald, H.R., Cumano, A., and Golub, R. (2016). Single-Cell Gene Expression
646 Analyses Reveal Heterogeneous Responsiveness of Fetal Innate Lymphoid Progenitors to
647 Notch Signaling. Cell Rep *14*, 1500-1516.

648 Cherrier, D.E., Serafini, N., and Di Santo, J.P. (2018). Innate Lymphoid Cell Development: A T
649 Cell Perspective. Immunity *48*, 1091-1103.

650 Cherrier, M., Sawa, S., and Eberl, G. (2012). Notch, Id2, and RORgammat sequentially
651 orchestrate the fetal development of lymphoid tissue inducer cells. J Exp Med *209*, 729-740.

652 Ciofani, M., Knowles, G.C., Wiest, D.L., von Boehmer, H., and Zuniga-Pflucker, J.C. (2006).
653 Stage-specific and differential notch dependency at the alphabeta and gammadelta T lineage
654 bifurcation. Immunity *25*, 105-116.

655 Constantinides, M.G., McDonald, B.D., Verhoef, P.A., and Bendelac, A. (2014). A committed
656 precursor to innate lymphoid cells. Nature *508*, 397-401.
657 De Obaldia, M.E., and Bhandoola, A. (2015). Transcriptional regulation of innate and adaptive
658 lymphocyte lineages. Annual review of immunology *33*, 607-642.
659 Dunon, D., Courtois, D., Vainio, O., Six, A., Chen, C.H., Cooper, M.D., Dangy, J.P., and Imhof,
660 B.A. (1997). Ontogeny of the immune system: gamma/delta and alpha/beta T cells migrate from
661 thymus to the periphery in alternating waves. J Exp Med *186*, 977-988.
662 Eberl, G., Colonna, M., Di Santo, J.P., and McKenzie, A.N. (2015). Innate lymphoid cells. Innate
663 lymphoid cells: a new paradigm in immunology. Science *348*, aaa6566.
664 Eberl, G., Marmon, S., Sunshine, M.J., Rennert, P.D., Choi, Y., and Littman, D.R. (2004). An
665 essential function for the nuclear receptor RORgamma(t) in the generation of fetal lymphoid
666 tissue inducer cells. Nat Immunol *5*, 64-73.
667 Fang, D., and Zhu, J. (2017). Dynamic balance between master transcription factors
668 determines the fates and functions of CD4 T cell and innate lymphoid cell subsets. J Exp Med
669 *214*, 1861-1876.
670 Garbe, A.I., Krueger, A., Gounari, F., Zuniga-Pflucker, J.C., and von Boehmer, H. (2006).
671 Differential synergy of Notch and T cell receptor signaling determines alphabeta versus
672 gammadelta lineage fate. J Exp Med *203*, 1579-1590.
673 Ghaedi, M., Shen, Z.Y., Orangi, M., Martinez-Gonzalez, I., Wei, L., Lu, X., Das, A., Heravi-
674 Moussavi, A., Marra, M.A., Bhandoola, A.*, et al.* (2020). Single-cell analysis of RORalpha tracer
675 mouse lung reveals ILC progenitors and effector ILC2 subsets. J Exp Med *217*.
676 Harly, C., Kenney, D., Ren, G., Lai, B., Raabe, T., Yang, Q., Cam, M.C., Xue, H.H., Zhao, K.,
677 and Bhandoola, A. (2019). The transcription factor TCF-1 enforces commitment to the innate
678 lymphoid cell lineage. Nat Immunol *20*, 1150-1160.
679 Hepworth, M.R., Monticelli, L.A., Fung, T.C., Ziegler, C.G., Grunberg, S., Sinha, R., Mantegazza,
680 A.R., Ma, H.L., Crawford, A., Angelosanto, J.M.*, et al.* (2013). Innate lymphoid cells regulate
681 CD4+ T-cell responses to intestinal commensal bacteria. Nature *498*, 113-117.
682 Ho, I.C., Tai, T.S., and Pai, S.Y. (2009). GATA3 and the T-cell lineage: essential functions before
683 and after T-helper-2-cell differentiation. Nat Rev Immunol *9*, 125-135.
684 Hoorweg, K., Peters, C.P., Cornelissen, F., Aparicio-Domingo, P., Papazian, N., Kazemier, G.,
685 Mjosberg, J.M., Spits, H., and Cupedo, T. (2012). Functional Differences between Human
686 NKp44(-) and NKp44(+) RORC(+) Innate Lymphoid Cells. Front Immunol *3*, 72.
687 Hosokawa, H., and Rothenberg, E.V. (2021). How transcription factors drive choice of the T cell
688 fate. Nat Rev Immunol *21*, 162-176.
689 Ishizuka, I.E., Chea, S., Gudjonson, H., Constantinides, M.G., Dinner, A.R., Bendelac, A., and
690 Golub, R. (2016). Single-cell analysis defines the divergence between the innate lymphoid cell
691 lineage and lymphoid tissue-inducer cell lineage. Nat Immunol *17*, 269-276.
692 Jassinskaja, M., Johansson, E., Kristiansen, T.A., Akerstrand, H., Sjoholm, K., Hauri, S.,
693 Malmstrom, J., Yuan, J., and Hansson, J. (2017). Comprehensive Proteomic Characterization
694 of Ontogenic Changes in Hematopoietic Stem and Progenitor Cells. Cell Rep *21*, 3285-3297.
695 Jones, R., Cosway, E.J., Willis, C., White, A.J., Jenkinson, W.E., Fehling, H.J., Anderson, G.,
696 and Withers, D.R. (2018). Dynamic changes in intrathymic ILC populations during murine
697 neonatal development. Eur J Immunol *48*, 1481-1491.
698 Kim, I., Saunders, T.L., and Morrison, S.J. (2007). Sox17 dependence distinguishes the

699 transcriptional regulation of fetal from adult hematopoietic stem cells. Cell *130*, 470-483.
700 Kiss, E.A., Vonarbourg, C., Kopfmann, S., Hobeika, E., Finke, D., Esser, C., and Diefenbach,
701 A. (2011). Natural aryl hydrocarbon receptor ligands control organogenesis of intestinal
702 lymphoid follicles. Science *334*, 1561-1565.
703 Klose, C.S.N., Flach, M., Mohle, L., Rogell, L., Hoyler, T., Ebert, K., Fabiunke, C., Pfeifer, D.,
704 Sexl, V., Fonseca-Pereira, D.*, et al.* (2014). Differentiation of type 1 ILCs from a common
705 progenitor to all helper-like innate lymphoid cell lineages. Cell *157*, 340-356.
706 Krishnamurty, A.T., and Turley, S.J. (2020). Lymph node stromal cells: cartographers of the
707 immune system. Nat Immunol *21*, 369-380.
708 Lee, J.S., Cella, M., McDonald, K.G., Garlanda, C., Kennedy, G.D., Nukaya, M., Mantovani, A.,
709 Kopan, R., Bradfield, C.A., Newberry, R.D.*, et al.* (2012). AHR drives the development of gut
710 ILC22 cells and postnatal lymphoid tissues via pathways dependent on and independent of
711 Notch. Nat Immunol *13*, 144-151.
712 Li, S., Bostick, J.W., Ye, J., Qiu, J., Zhang, B., Urban, J.F., Jr., Avram, D., and Zhou, L. (2018).
713 Aryl Hydrocarbon Receptor Signaling Cell Intrinsically Inhibits Intestinal Group 2 Innate
714 Lymphoid Cell Function. Immunity *49*, 915-928 e915.
715 Li, S., Heller, J.J., Bostick, J.W., Lee, A., Schjerven, H., Kastner, P., Chan, S., Chen, Z.E., and
716 Zhou, L. (2016). Ikaros Inhibits Group 3 Innate Lymphoid Cell Development and Function by
717 Suppressing the Aryl Hydrocarbon Receptor Pathway. Immunity *45*, 185-197.
718 Lim, A.I., and Di Santo, J.P. (2019). ILC-poiesis: Ensuring tissue ILC differentiation at the right
719 place and time. Eur J Immunol *49*, 11-18.
720 Lim, A.I., Li, Y., Lopez-Lastra, S., Stadhouders, R., Paul, F., Casrouge, A., Serafini, N., Puel, A.,
721 Bustamante, J., Surace, L.*, et al.* (2017). Systemic Human ILC Precursors Provide a Substrate
722 for Tissue ILC Differentiation. Cell *168*, 1086-1100 e1010.
723 Lyu, M., Suzuki, H., Kang, L., Gaspal, F., Zhou, W., Goc, J., Zhou, L., Zhou, J., Zhang, W., Bank,
724 J.R.I.L.C.*, et al.* (2022). ILC3s select microbiota-specific regulatory T cells to establish tolerance
725 in the gut. Nature *610*, 744-751.
726 Mao, K., Baptista, A.P., Tamoutounour, S., Zhuang, L., Bouladoux, N., Martins, A.J., Huang, Y.,
727 Gerner, M.Y., Belkaid, Y., and Germain, R.N. (2018). Innate and adaptive lymphocytes
728 sequentially shape the gut microbiota and lipid metabolism. Nature *554*, 255-259.
729 Medvinsky, A., Rybtsov, S., and Taoudi, S. (2011). Embryonic origin of the adult hematopoietic
730 system: advances and questions. Development *138*, 1017-1031.
731 Oherle, K., Acker, E., Bonfield, M., Wang, T., Gray, J., Lang, I., Bridges, J., Lewkowich, I., Xu,
732 Y., Ahlfeld, S.*, et al.* (2020). Insulin-like Growth Factor 1 Supports a Pulmonary Niche that
733 Promotes Type 3 Innate Lymphoid Cell Development in Newborn Lungs. Immunity *52*, 275-294
734 e279.
735 Onder, L., and Ludewig, B. (2018). A Fresh View on Lymph Node Organogenesis. Trends
736 Immunol *39*, 775-787.
737 Possot, C., Schmutz, S., Chea, S., Boucontet, L., Louise, A., Cumano, A., and Golub, R. (2011).
738 Notch signaling is necessary for adult, but not fetal, development of RORgammat(+) innate
739 lymphoid cells. Nat Immunol *12*, 949-958.
740 Qiu, X., Zhang, Y., Martin-Rufino, J.D., Weng, C., Hosseinzadeh, S., Yang, D., Pogson, A.N.,
741 Hein, M.Y., Hoi Joseph Min, K., Wang, L.*, et al.* (2022). Mapping transcriptomic vector fields of
742 single cells. Cell *185*, 690-711 e645.

743 Ren, G., Lai, B., Harly, C., Baek, S., Ding, Y., Zheng, M., Cao, Y., Cui, K., Yang, Y., Zhu, J.*, et*
744 *al.* (2022). Transcription factors TCF-1 and GATA3 are key factors for the epigenetic priming of
745 early innate lymphoid progenitors toward distinct cell fates. Immunity *55*, 1402-1413 e1404.
746 Rothenberg, E.V. (2019). Programming for T-lymphocyte fates: modularity and mechanisms.
747 Genes Dev *33*, 1117-1135.
748 Sanos, S.L., Bui, V.L., Mortha, A., Oberle, K., Heners, C., Johner, C., and Diefenbach, A. (2009).
749 RORgammat and commensal microflora are required for the differentiation of mucosal
750 interleukin 22-producing NKp46+ cells. Nat Immunol *10*, 83-91.
751 Sawa, S., Cherrier, M., Lochner, M., Satoh-Takayama, N., Fehling, H.J., Langa, F., Di Santo,
752 J.P., and Eberl, G. (2010). Lineage relationship analysis of RORgammat+ innate lymphoid cells.
753 Science *330*, 665-669.
754 Schjerven, H. (2013). Selective regulation of lymphopoiesis and leukemogenesis by individual
755 zinc fingers of Ikaros. Nat Immunol *4*, 1073-1085.
756 Tanigaki, K., Tsuji, M., Yamamoto, N., Han, H., Tsukada, J., Inoue, H., Kubo, M., and Honjo, T.
757 (2004). Regulation of alphabeta/gammadelta T cell lineage commitment and peripheral T cell
758 responses by Notch/RBP-J signaling. Immunity *20*, 611-622.
759 Vivier, E., Artis, D., Colonna, M., Diefenbach, A., Di Santo, J.P., Eberl, G., Koyasu, S., Locksley,
760 R.M., McKenzie, A.N.J., Mebius, R.E.*, et al.* (2018). Innate Lymphoid Cells: 10 Years On. Cell
761 *174*, 1054-1066.
762 Vonarbourg, C., Mortha, A., Bui, V.L., Hernandez, P.P., Kiss, E.A., Hoyler, T., Flach, M.,
763 Bengsch, B., Thimme, R., Holscher, C.*, et al.* (2010). Regulated expression of nuclear receptor
764 RORgammat confers distinct functional fates to NK cell receptor-expressing RORgammat(+)
765 innate lymphocytes. Immunity *33*, 736-751.
766 Walker, J.A., Barlow, J.L., and McKenzie, A.N. (2013). Innate lymphoid cells--how did we miss
767 them? Nature reviews Immunology *13*, 75-87.
768 Wong, S.H., Walker, J.A., Jolin, H.E., Drynan, L.F., Hams, E., Camelo, A., Barlow, J.L., Neill,
769 D.R., Panova, V., Koch, U.*, et al.* (2012). Transcription factor RORalpha is critical for nuocyte
770 development. Nat Immunol *13*, 229-236.
771 Yagi, R., Zhong, C., Northrup, D.L., Yu, F., Bouladoux, N., Spencer, S., Hu, G., Barron, L.,
772 Sharma, S., Nakayama, T.*, et al.* (2014). The transcription factor GATA3 is critical for the
773 development of all IL-7Ralpha-expressing innate lymphoid cells. Immunity *40*, 378-388.
774 Yang, Q., Li, F., Harly, C., Xing, S., Ye, L., Xia, X., Wang, H., Wang, X., Yu, S., Zhou, X.*, et al.*
775 (2015). TCF-1 upregulation identifies early innate lymphoid progenitors in the bone marrow.
776 Nat Immunol *16*, 1044-1050.
777 Yu, Y., Tsang, J.C.H., Wang, C., Clare, S., Wang, J., Chen, X., Brandt, C., Kane, L., Campos,
778 L.S., Lu, L.*, et al.* (2016). Single-cell RNA-seq identifies a PD-1hi ILC progenitor and defines
779 its development pathway. Nature *539*, 102-106.
780 Yuan, J., Nguyen, C.K., Liu, X., Kanellopoulou, C., and Muljo, S.A. (2012). Lin28b reprograms
781 adult bone marrow hematopoietic progenitors to mediate fetal-like lymphopoiesis. Science *335*,
782 1195-1200.
783 Zeis, P., Lian, M., Fan, X., Herman, J.S., Hernandez, D.C., Gentek, R., Elias, S., Symowski, C.,
784 Knopper, K., Peltokangas, N.*, et al.* (2020). In Situ Maturation and Tissue Adaptation of Type 2
785 Innate Lymphoid Cell Progenitors. Immunity *53*, 775-792 e779.
786 Zhong, C., Cui, K., Wilhelm, C., Hu, G., Mao, K., Belkaid, Y., Zhao, K., and Zhu, J. (2015).

Group 3 innate lymphoid cells continuously require the transcription factor GATA-3 after commitment. Nature Immunology.

Zhong, C., Zheng, M., Cui, K., Martins, A.J., Hu, G., Li, D., Tessarollo, L., Kozlov, S., Keller, J.R., Tsang, J.S.*, et al.* (2020). Differential Expression of the Transcription Factor GATA3 Specifies Lineage and Functions of Innate Lymphoid Cells. Immunity *52*, 83-95 e84.

Figures

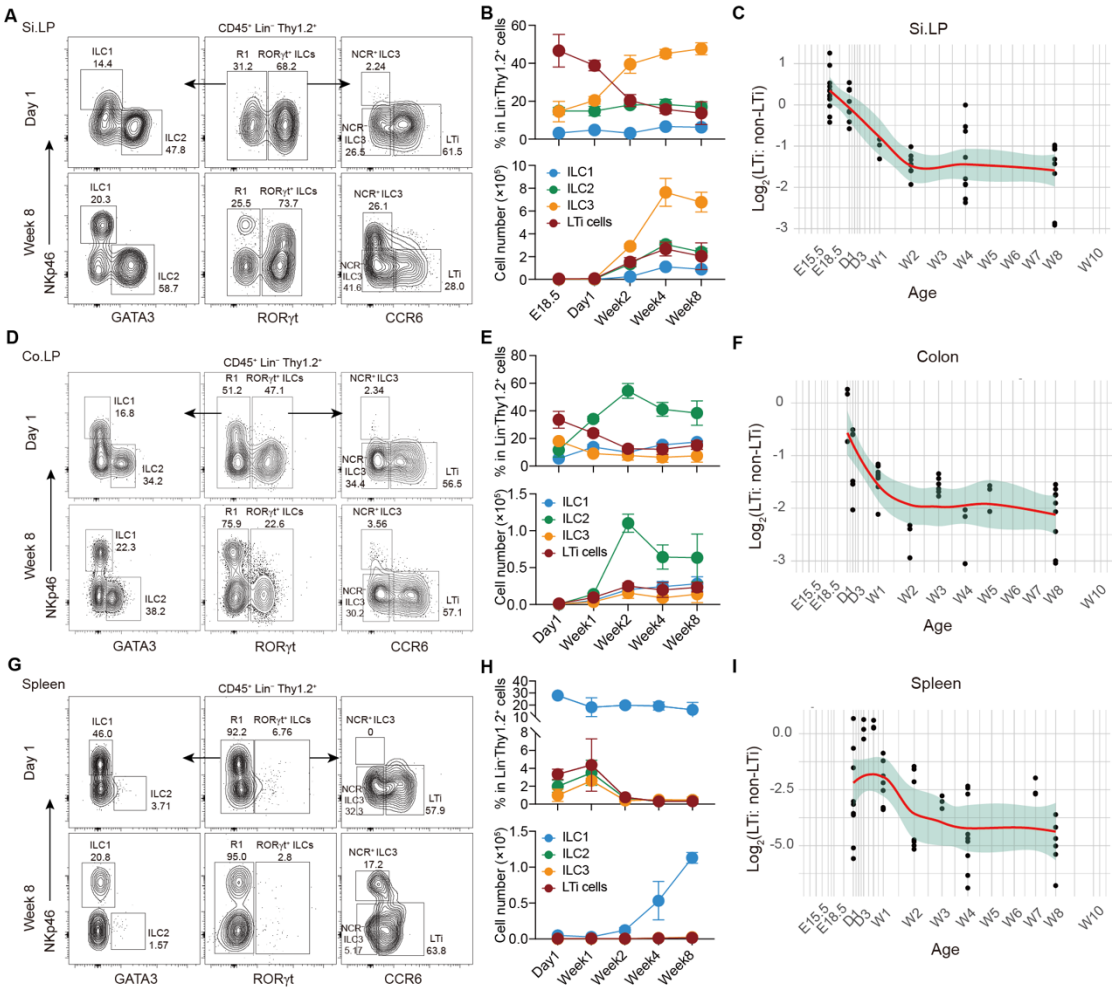

Figure 1 Temporal and tissue distribution of innate lymphoid cells during ontogeny

(A, D and G) Representative FACS plots show the frequencies of major ILC subsets in (A) lamina propria of small intestine (Si.LP), (D) lamina propria of colon (Co.LP) and (G) spleen, between newborn (Day 1) and adult (Week 8) mice.

(B, E and H) The percentage and absolute number of ILC subsets in (B) Si.LP, (E) Co.LP and (H) spleen during ontogeny are shown. Data (n=3-6 mice per group) represent two independent experiments (mean ± SD).

(C, F, I) The logarithm of the percentage ratio of LTi cells to non-LTi ILCs in (C) Si.LP, (F) Co.LP, and (I) spleen are plotted. Each dot represents the value for one individual mouse.

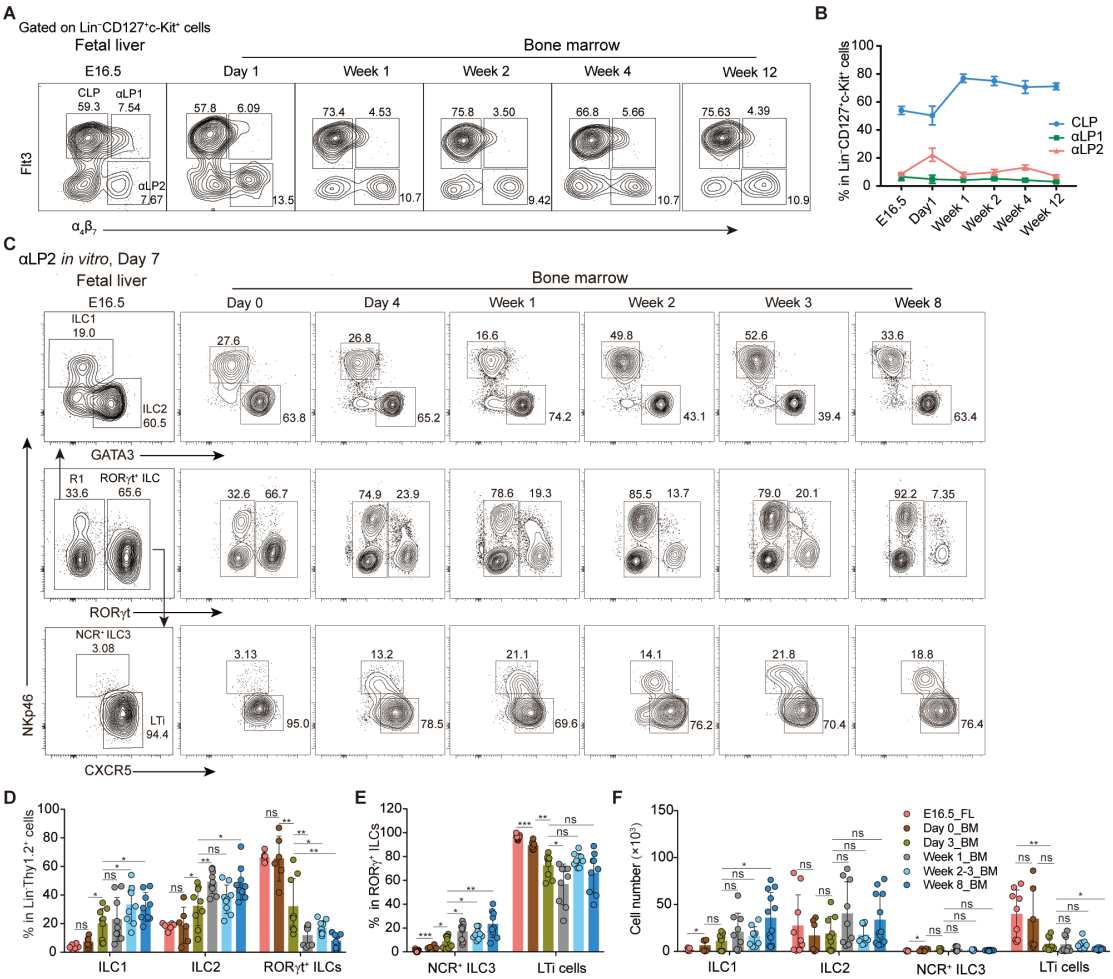

Figure 2 ILC subsets generated by progenitors from different stages during ontogeny

(A) CD45⁺Lin⁻CD127⁺c-Kit$^{int/+}$ cells were gated to identify CLP, αLP1, and αLP2 in fetal liver (E16.5) and bone marrow at neonatal (Day 1), infant (Day 4, Week 1, and Week 2), weaning (Week 4), and adult stages (Week 12).

(B) Dynamic percentages of CLPs, αLP1s, and αLP2s during ontogeny. Data (n=10 mice per group) are pooled from two independent experiments (mean ± SD).

(C) Representative FACS plots show ILC subsets derived from αLP2s sorted from fetal liver (E16.5), or bone marrow at the newborn (Day 0), infant (Day 4 and Week 1), weaning (Week 2-3) and adult mice (Week 8), after 7 days of *in vitro* culture with IL-7 and SCF.

(D-F) Percentage (D-E) and absolute cell number (F) of major ILC subsets in (C). Data (n=6-15 per group) are pooled from three independent experiments (mean ± SD).

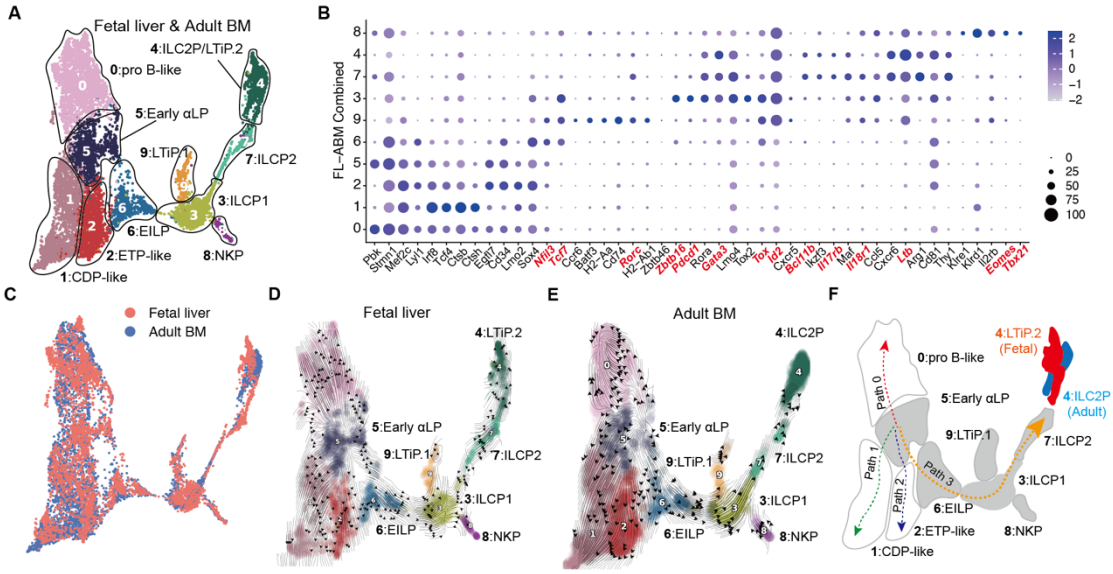

Figure 3 ILC differentiation trajectories in fetal liver and adult bone marrow revealed by single-cell RNA-sequencing analysis.

(A) The cellular composition of αLPs from integrated fetal liver and adult bone marrow is visualized using Uniform Manifold Approximation and Projection (UMAP). Cell types are color-coded.

(B) Feature gene expression is shown across the identified clusters among αLPs using dot-plot analyses.

(C) The integrated UMAP shows αLPs from fetal liver (red) and adult bone marrow (blue).

(D and E) RNA velocity algorithm-derived transition probabilities projected onto UMAP plots of (D) fetal liver and (E) adult bone marrow αLPs. Streamlines represent averaged and projected RNA velocities.

(F) Schematic diagram showing the potential ILC differentiation trajectories in fetal liver and adult bone marrow.

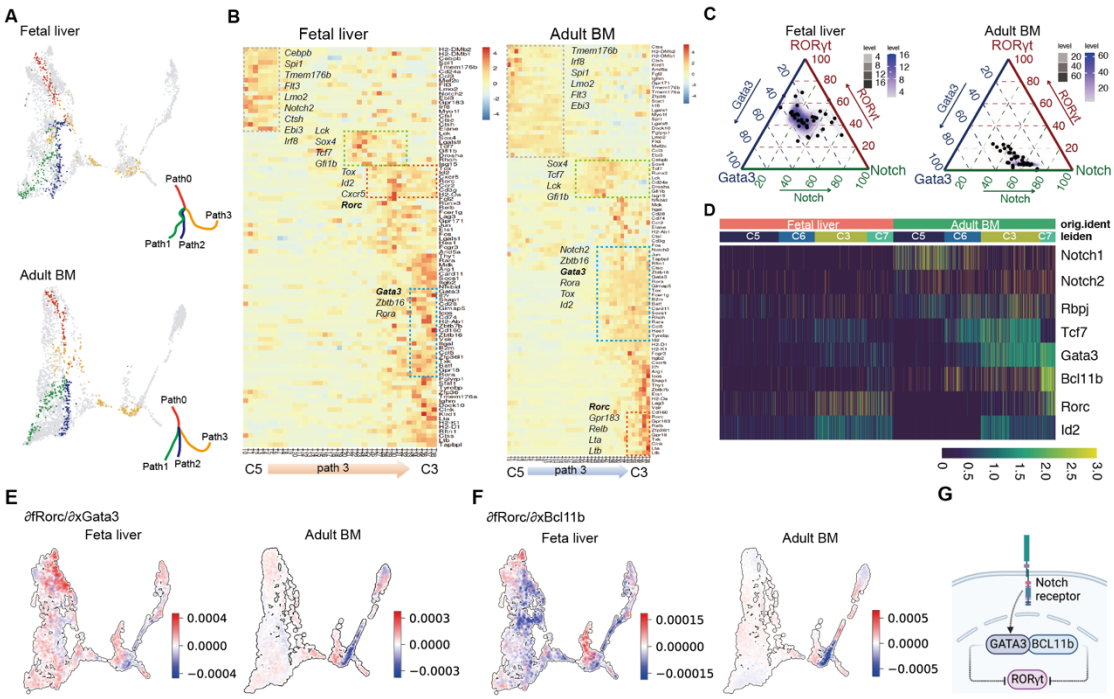

Figure 4 Comparation of gene programs during fetal and adult ILC development

(A) Visualization of the representative cells along the paths revealed in fetal liver and adult bone marrow αLPs.

(B) Heatmaps displaying differentially expressed genes along the ILC differentiation pseudotime (path 3) from early αLP1s (C5) to ILCPs (C3) in fetal liver and adult bone marrow.

(C) Analysis of targeted genes by Notch signaling, GATA3, or RORγt along ILC differentiation pseudotime (path 3) in both fetal liver and adult bone marrow. Ternary plots showing that cells closer to an outer edge or apex were more likely associated with higher activation of the indicated transcription factor.

(D) Transcription of genes associated with Notch signaling, *Gata3*, *Bcl11b*, and *Rorc* during both fetal and adult ILC differentiation.

(E and F) *Dynamo* analysis predicting the potential relationship between (E) *Rorc* and *Gata3*, as well as between (F) *Rorc* and *Bcl11b* during fetal and adult ILC development trajectories.

(G) Schematic diagram showing the potential relationship among Notch signaling, GATA3/BCL11b and RORγt.

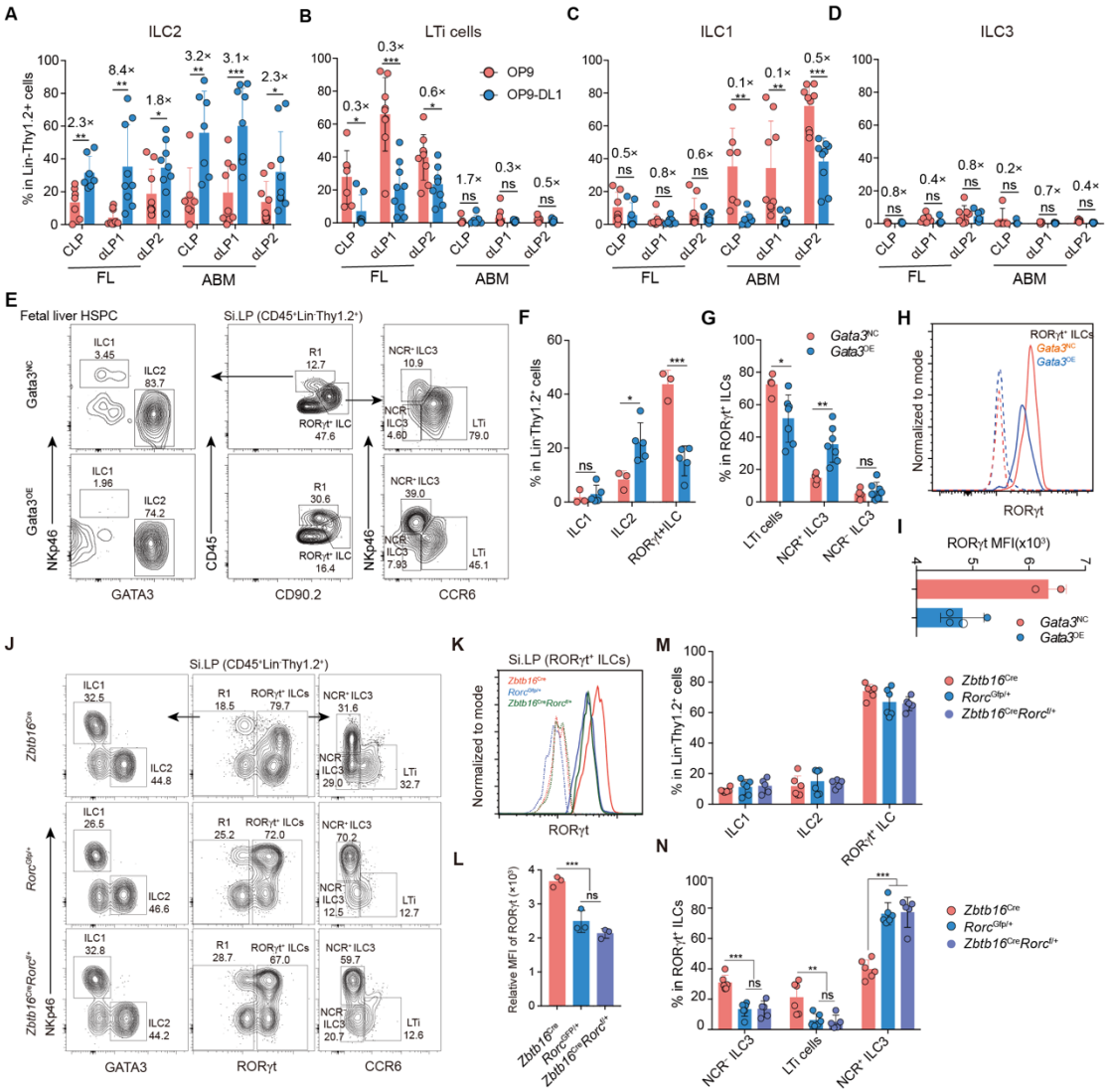

Figure 5 Enhanced Notch signaling, GATA3 and decreased RORγt suppresses LTi cell differentiation.

(A-D) Percentage of ILC1s, ILC2s, ILC3 and LTi cells derived from fetal and adult CLPs, αLP1s and αLP2s after co-culture with either OP9 or OP9-DL1 stromal cells *in vitro*. Data (n=7-8 mice per group) are pooled from three to four independent experiments (mean ± SD).

(E) Representative flow cytometry plots showing the ILC subsets derived *in vivo* from the fetal liver progenitors transduced with either empty plasmid (*Gata3*^{NC}) or *Gata3* overexpression (*Gata3*^{OE}) in the recipient intestine.

(F-G) The percentage of ILC subsets in (E). Data (n=3-7 mice per group) are pooled from two independent experiments (mean ± SD).

(H and I) Intracellular staining of RORγt in RORγt^{+} ILCs in (G). Data (n= 2-3 mice per group) represent two independent experiments (mean ± SD).

(J) Flow cytometry analysis showing the major ILC subsets in the small intestine of *Rorc* heterozygous mice, including both *Rorc*$^{Gfp/+}$ and *Zbtb16*^{Cre}*Rorc*$^{f/+}$ mice.

(K and L) Mean fluorescence intensity (MFI) of RORγt in small intestinal RORγt^{+} ILCs from *Rorc* heterozygous mice. Data (n=3 per group) represent two independent experiments

(mean ± SD).

(M and N) Percentage of major ILC subsets in the small intestine from *Rorc* heterozygous mice. Data (n=3 per group) represent two independent experiments (mean ± SD).